LHCb-CONF-2011-049
October 21, 2011

Tagged time-dependent angular analysis of $B_s^0 \to J/\psi\,\phi$ decays with 337 pb^{-1} at LHCb

The LHCb Collaboration[1]

Abstract

The interference between B_s^0 decays to $J/\psi\,\phi$ either directly or via B_s^0–$\overline{B}_s^0$ oscillation gives rise to a CP violating phase $\phi_s^{J/\psi\,\phi}$. Using a sample of 8276 ± 94 $B_s^0 \to J/\psi\phi$ events extracted from 337 pb^{-1} of pp collisions collected during the 2011 LHC run at $\sqrt{s} = 7$ TeV, we fit for nine physics parameters, among which the phase $\phi_s^{J/\psi\,\phi}$, the decay width difference $\Delta\Gamma_s$ and the decay width Γ_s. For one of two ambiguous solutions ($\phi_s^{J/\psi\,\phi} \leftrightarrow \pi - \phi_s^{J/\psi\,\phi}$; $\Delta\Gamma_s \leftrightarrow -\Delta\Gamma_s$) we find

$$\begin{aligned}
\phi_s^{J/\psi\,\phi} &= 0.13 \pm 0.18\ (\text{stat}) \pm 0.07\ (\text{syst})\ \text{rad},\\
\Gamma_s &= 0.656 \pm 0.009\ (\text{stat}) \pm 0.008\ (\text{syst})\ \text{ps}^{-1},\\
\Delta\Gamma_s &= 0.123 \pm 0.029\ (\text{stat}) \pm 0.011\ (\text{syst})\ \text{ps}^{-1},
\end{aligned}$$

in good agreement with the Standard Model predictions. This is the most precise measurement of $\phi_s^{J/\psi\,\phi}$and Γ_s. Furthermore, it is the first direct experimental evidence of a non-zero value of $\Delta\Gamma_s$.

[1]Conference report prepared for *Lepton Photon*, Mumbai, 22nd August 2011. Contact authors: Stephanie Hansmann-Menzemer and Wouter Hulsbergen

1 Introduction

Decays of neutral B mesons provide a laboratory to study CP-violation originating from a non-trivial complex phase in the CKM matrix [1]. The relative phase between the direct decay amplitude and the amplitude of decay via oscillation gives rise to time-dependent CP-violation, a difference in the decay time distribution of B-meson and anti-B-meson decays [2]. The decay $B_s^0 \to J/\psi\phi$ is considered the golden mode for measuring this type of CP-violation in the B_s^0 system. In the Standard Model the CP-violating phase in this decay is predicted to be $\phi_s^{J/\psi\,\phi} \simeq -2\beta_s$, where $\beta_s = \arg\left(-V_{ts}V_{tb}^*/V_{cs}V_{cb}^*\right)$ [3]. The indirect determination via global fits to experimental data gives $2\beta_s = (0.0363^{+0.0016}_{-0.0015})\,\text{rad}$ [4].

Measurements on B_d^0 decays performed by the B factories severely constrain any beyond the Standard Model contributions to decays via tree topologies or in $B_d^0 - \bar{B}_d^0$ mixing. However, new contributions to $B_s^0 - \bar{B}_s^0$ mixing [5, 6] are much less constrained and may alter the expected value of $\phi_s^{J/\psi\,\phi}$ [7]. Previous measurements of $\phi_s^{J/\psi\,\phi}$ in $B_s^0 \to J/\psi\phi$ decays have been reported by the Tevatron experiments CDF [8] and DØ [9], using approximately 6 500 and 3 400 $B_s^0 \to J/\psi\phi$ candidates, respectively. For both experiments the uncertainty on $\phi_s^{J/\psi\,\phi}$ is about 0.5 rad. DØ recently updated this result and obtained $\phi_s^{J/\psi\,\phi} = -0.56^{+0.36}_{-0.32}\,\text{rad}$ with $\sim 5\,000$ signal candidates [10].

In spring 2010 the LHCb collaboration presented its first measurement of $\phi_s^{J/\psi\,\phi}$ based on about 840 $B_s^0 \to J/\psi\phi$ decays extracted from $36\,\text{pb}^{-1}$ of pp collisions collected during the 2010 LHC run at $\sqrt{s} = 7\,\text{TeV}$ [11]. The obtained precision for $\phi_s^{J/\psi\,\phi}$ was about 1.1 rad. In this document we present an update of this analysis using a sample that contains 8276 ± 94 $B_s^0 \to J/\psi\phi$ decays, extracted from $337\,\text{pb}^{-1}$ of pp collisions. We will frequently refer to the work described in [11] and to the corresponding supporting conference notes. The different steps of the analysis are described in Section 2 and the results reported in Section 3.

2 Description of the analysis

The event selection is described in [12]. There have been only minor changes with respect to this selection for the J/ψ mass and vertex χ^2 cut. The selected event sample is dominated by a large background with several distinct contributions:

- random combinations of four prompt tracks;
- background from prompt J/ψ events, combined with two random tracks;
- background with large reconstructed decay time due to J/ψ from non-signal $B \to J/\psi\, X$ decays;
- combinatorial background with large reconstructed decay time, where the two reconstructed muons originate from semi-leptonic B and D decays;

In order to reduce the sensitivity of the fit to the description of the prompt contribution only events with decay time $t > 0.3$ ps are considered in this analysis. At total of 8276 ± 94 $B_s^0 \to J/\psi\phi$ decays are left after the full selection. The remaining background in the sample is only of the order of a few percent. The invariant mass distribution of the selected events is shown in Fig. 1.

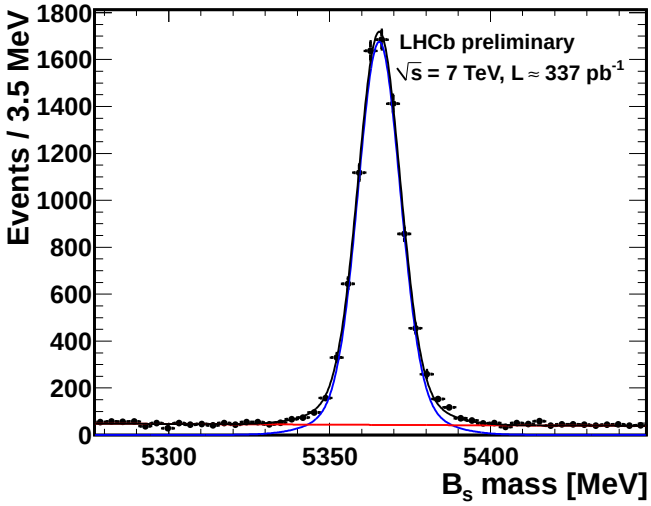

Figure 1: Reconstructed invariant mass distribution of selected $B_s^0 \to J/\psi\phi$ candidates. The superimposed blue curve is the signal contribution. The red curve corresponds to the combinatorial background. The black curve describes sum of signal and background candidates.

The phase $\phi_s^{J/\psi\phi}$ is extracted from the data with an unbinned maximum likelihood fit to the candidate invariant mass m, the decay time t, the initial B_s^0 flavour d and the 4-body decay angles in the transversity frame $\Omega = \{\cos\theta, \varphi, \cos\psi\}$, defined in [13] and illustrated in Fig. 2.

A major systematic uncertainty in the $\phi_s^{J/\psi\phi}$ analysis performed with data taken in 2010 [11] arose from neglecting potential S-wave contribution to the signal [14, 15]. In the current analysis the S-wave contribution is included in the likelihood fit. Apart from this the fitting formalism is identical to the previous analysis.

2.1 The signal PDF

The likelihood function for N events can be written generically as

$$\mathcal{L} = \prod_e^N \mathcal{P}\left(\{m, t, \Omega, d, \omega\}_e; \lambda_{\rm phys}, \lambda_{\rm det}, \lambda_{\rm bkg}\right) , \tag{1}$$

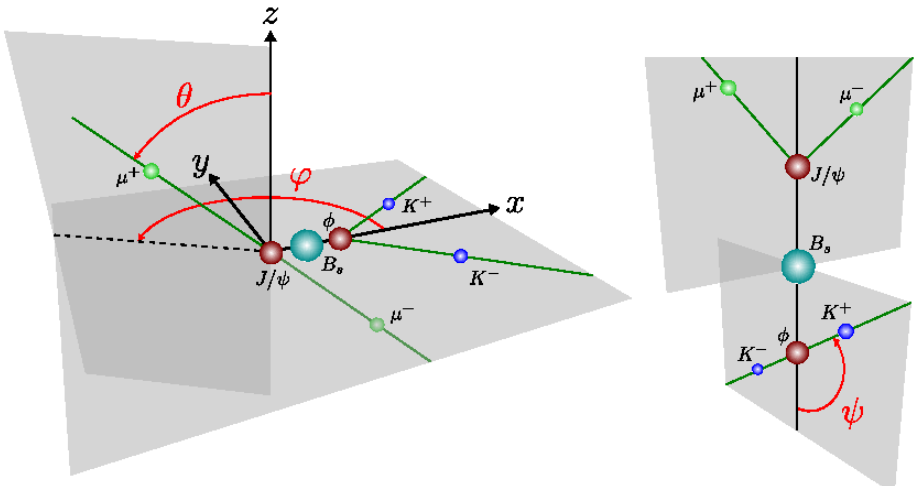

Figure 2: Definition of the decay angles in the transversity frame: θ is the angle formed by the positive lepton (ℓ^+) and the z axis, in the J/ψ rest frame. The angle φ is the azimuthal angle of ℓ^+ in the same frame. In the ϕ meson rest frame, ψ is the angle between $\vec{p}(K^+)$ and $-\vec{p}(J/\psi)$.

where the probability density function (PDF) $\mathcal{P}$ consists of a signal component $\mathcal{S}$ and a background component $\mathcal{B}$,

$$\mathcal{P} = f_{\rm sig}\,\mathcal{S} + (1 - f_{\rm sig})\,\mathcal{B}\,, \tag{2}$$

with $f_{\rm sig}$ the signal fraction. The set of physics parameters $\lambda_{\rm phys}$ includes the average B_s^0 decay width Γ_s, the decay width difference between the B_s^0 mass eigenstates $\Delta\Gamma_s$, the oscillation frequency Δm_s, the CP violating phase $\phi_s^{J/\psi\,\phi}$ and the complex angular amplitudes at $t = 0$, denoted by $A_0(0)$, $A_\parallel(0)$ and $A_\perp(0)$ for the P-wave and by $A_s(0)$ for the S-wave. In the likelihood fit we remove one arbitrary phase by choosing $A_0(0)$ real and we normalize the amplitudes such that $|A_\parallel|^2 = 1 - |A_\perp(0)|^2 - |A_0(0)|^2 - |A_s(0)|^2$.

The symbol $\lambda_{\rm det}$ represents the parameters involved in describing resolutions, acceptance and flavour tag calibration. The parameters used to describe the background are generically denoted by $\lambda_{\rm bkg}$.

We have verified that the candidate mass m does not correlate with the other observables such that the PDF can be factorized. The invariant mass distribution for signal candidates is described by a sum of two Gaussian distributions with common mean. The relative fractions and the ratio of the widths of the two Gaussians are fixed from Monte Carlo simulation, while the mean and one parameter for the width are extracted from the data. The invariant mass distribution for background candidates is described by an exponential.

We have also verified that for $t > 0$ the decay time and the decay angle distributions of the background are uncorrelated and do not depend on the flavour tag. The background decay time distribution is described by two exponentials with different lifetimes. The

relative contribution and the lifetime parameters of the exponentials are floating in the fit. For the description of the angular distribution of the background we have used 3D polynomials fitted to the mass sideband [16]. As an alternative we have used a PDF with constant density in the three decay angles and assigned the difference in the results as a systematic uncertainty.

In the following we concentrate on the PDF for signal candidates only. Ignoring detector effects, the distribution for the decay time t and the transversity angles Ω for initial B_s^0 decaying into $J/\psi\,\phi$ is given by the differential decay rate

$$\frac{\mathrm{d}^4\Gamma(B_s^0 \to J/\psi\phi)}{\mathrm{d}t\;\mathrm{d}\cos\theta\;\mathrm{d}\varphi\;\mathrm{d}\cos\psi} \equiv \frac{\mathrm{d}^4\Gamma}{\mathrm{d}t\;\mathrm{d}\Omega} \propto \sum_{k=1}^{10} h_k(t) f_k(\Omega)\,. \tag{3}$$

The ten time-dependent amplitudes $h_k(t)$ and the angular functions $f_k(\Omega)$ are defined as

k	$h_k(t)$	$f_k(\theta,\psi,\varphi)$
1	$\lvert A_0\rvert^2(t)$	$2\cos^2\psi\,(1-\sin^2\theta\cos^2\phi)$
2	$\lvert A_\parallel(t)\rvert^2$	$\sin^2\psi\,(1-\sin^2\theta\sin^2\phi)$
3	$\lvert A_\perp(t)\rvert^2$	$\sin^2\psi\sin^2\theta$
4	$\Im(A_\parallel(t)\,A_\perp(t))$	$-\sin^2\psi\sin 2\theta\sin\phi$
5	$\Re(A_0(t)\,A_\parallel(t))$	$\frac{1}{2}\sqrt{2}\,\sin 2\psi\sin^2\theta\sin 2\phi$
6	$\Im(A_0(t)\,A_\perp(t))$	$\frac{1}{2}\sqrt{2}\,\sin 2\psi\sin 2\theta\cos\phi$
7	$\lvert A_s(t)\rvert^2$	$\frac{2}{3}(1-\sin^2\theta\cos^2\phi)$
8	$\Re(A_s^*(t)A_\parallel(t))$	$\frac{1}{3}\sqrt{6}\sin\psi\sin^2\theta\sin 2\phi$
9	$\Im(A_s^*(t)A_\perp(t))$	$\frac{1}{3}\sqrt{6}\sin\psi\sin 2\theta\cos\phi$
10	$\Re(A_s^*(t)A_0(t))$	$\frac{4}{3}\sqrt{3}\cos\psi(1-\sin^2\theta\cos^2\phi)$

The terms 7–10 are related to the description of the S-wave component. We ignore the effects of CP violation in B_s^0 mixing and in the decay amplitudes, which are expected to be small. Expressed in terms of the size $|A_i(0)|$ and phase δ_i of the transversity and

S-wave amplitudes at $t = 0$, the time dependent amplitudes are then given by

$$
\begin{aligned}
|A_0|^2(t) &= |A_0|^2 e^{-\Gamma_s t}[\cosh\left(\frac{\Delta\Gamma}{2}t\right) - \cos\phi_s \sinh\left(\frac{\Delta\Gamma}{2}t\right) + \sin\phi_s \sin(\Delta m t)]\,, && (4)\\
|A_\parallel(t)|^2 &= |A_\parallel|^2 e^{-\Gamma_s t}[\cosh\left(\frac{\Delta\Gamma}{2}t\right) - \cos\phi_s \sinh\left(\frac{\Delta\Gamma}{2}t\right) + \sin\phi_s \sin(\Delta m t)]\,, && (5)\\
|A_\perp(t)|^2 &= |A_\perp|^2 e^{-\Gamma_s t}[\cosh\left(\frac{\Delta\Gamma}{2}t\right) + \cos\phi_s \sinh\left(\frac{\Delta\Gamma}{2}t\right) - \sin\phi_s \sin(\Delta m t)]\,, && (6)\\
\Im(A_\parallel(t)\, A_\perp(t)) &= |A_\parallel||A_\perp| e^{-\Gamma_s t}[-\cos(\delta_\perp - \delta_\parallel)\sin\phi_s \sinh\left(\frac{\Delta\Gamma}{2}t\right)\\
&\quad - \cos(\delta_\perp - \delta_{-\parallel})\cos\phi_s \sin(\Delta m t) + \sin(\delta_\perp - \delta_\parallel)\cos(\Delta m t)]\,, && (7)\\
\Re(A_0(t)\, A_\parallel(t)) &= |A_0||A_\parallel| e^{-\Gamma_s t}\cos(\delta_\parallel - \delta_0)[\cosh\left(\frac{\Delta\Gamma}{2}t\right) - \cos\phi_s \sinh\left(\frac{\Delta\Gamma}{2}t\right)\\
&\quad + \sin\phi_s \sin(\Delta m t)]\,, && (8)\\
\Im(A_0(t)\, A_\perp(t)) &= |A_0||A_\perp| e^{-\Gamma_s t}[-\cos(\delta_\perp - \delta_0)\sin\phi_s \sinh\left(\frac{\Delta\Gamma}{2}t\right)\\
&\quad - \cos(\delta_\perp - \delta_0)\cos\phi_s \sin(\Delta m t) + \sin(\delta_\perp - \delta_0)\cos(\Delta m t)]\,, && (9)\\
|A_s(t)|^2 &= |A_s|^2 e^{-\Gamma_s t}[\cosh\left(\frac{\Delta\Gamma}{2}t\right) + \cos\phi_s \sinh\left(\frac{\Delta\Gamma}{2}t\right) - \sin\phi_s \sin(\Delta m t]\,, && (10)\\
\Re(A_s^*(t) A_\parallel(t)) &= |A_s||A_\parallel| e^{-\Gamma_s t}[-\sin(\delta_\parallel - \delta_s)\sin\phi_s \sinh\left(\frac{\Delta\Gamma}{2}t\right) - \sin(\delta_\parallel - \delta_s)\ \cos\phi_s \sin(\Delta m t)\\
&\quad + \cos(\delta_\parallel - \delta_s)\cos(\Delta m t)]\,, && (11)\\
\Im(A_s^*(t) A_\perp(t)) &= |A_s||A_\perp| e^{-\Gamma_s t}\sin(\delta_\perp - \delta_s)[\cosh\left(\frac{\Delta\Gamma}{2}t\right) + \cos\phi_s \sinh\left(\frac{\Delta\Gamma}{2}t\right)\\
&\quad - \sin\phi_s \sin(\Delta m t)]\,, && (12)\\
\Re(A_s^*(t) A_0(t)) &= |A_s||A_0| e^{-\Gamma_s t}[-\sin(\delta_0 - \delta_s)\sin\phi_s \sinh\left(\frac{\Delta\Gamma}{2}t\right)\\
&\quad - \sin(\delta_0 - \delta_s)\cos\phi_s \sin(\Delta m t) + \cos(\delta_0 - \delta_s)\cos(\Delta m t)]\,. && (13)
\end{aligned}
$$

The decay time dependent decay rates for an initial $\overline{B_s^0}$ decaying to $J/\psi\,\phi$ can be obtained from those above by inserting a factor -1 in front of the terms involving mixing ($\sin(\Delta m_s t)$ and $\cos(\Delta m_s t)$).

The decay rates are invariant under the simultaneous transformation

$$
\begin{array}{rcl}
\phi_s & \longleftrightarrow & \pi - \phi_s \\
\Delta\Gamma_s & \longleftrightarrow & -\Delta\Gamma_s \\
\delta_\parallel & \longleftrightarrow & -\delta_\parallel \\
\delta_\perp & \longleftrightarrow & \pi - \delta_\perp\,.
\end{array}
\qquad (14)
$$

It is possible to resolve this two-fold ambiguity by measuring the phase of the S-wave contribution as function of invariant KK mass as discussed in [15]. However in the present analysis we only fit for an overall S-wave contribution and do not perform a mass dependent analysis.

2.2 Flavour tagging

The signal distributions are corrected for resolution and acceptance effects for both decay time and decay angles and for the dilution from flavour tagging. For the latter, we first divide the PDF into tagged and untagged events. The PDF for the tagged events is

obtained from the distributions in Equation 3 by inserting experimental dilutions in front of all terms involving the mixing

$$\begin{aligned} \sin(\Delta m_s t) &\longrightarrow d\,\mathcal{D}\,\sin(\Delta m_s t)\,, \\ \cos(\Delta m_s t) &\longrightarrow d\,\mathcal{D}\,\cos(\Delta m_s t)\,, \end{aligned} \tag{15}$$

where d is the initial flavour tag decision ($+1$ for B_s^0 and -1 for $\overline{B}_s^0$). The dilution is given by $\mathcal{D} = 1 - 2\omega$, where ω is the mistag probability. We assume that the flavour tagging performance does not depend on the decay time. For the untagged events $d = 0$ and all terms involving mixing are removed from Equation 3.

The strategy for the optimization and calibration of the flavour tagging is described in detail in [17] based on data collected in 2010. The same calibration approach was applied on the 2011 data set used for the analysis presented here. In this analysis we exploit only the "opposite-side" (OS) flavour taggers. The OS flavour tagger uses four different signatures, namely high p_T muons, electrons and kaons, and the net charge of an inclusively reconstructed secondary vertex. The combination procedure provides an estimated per-event mistag probability. It is calibrated with $B^+ \to J/\psi\, K^+$ decays, which provide a priori known flavour, assuming a linear dependence between the estimated mistag probability η_c and the actual mistag probability ω (Fig 3 (left))

$$\omega \;=\; p_0 \;+\; p_1\,(\eta_c - \langle\eta_c\rangle)\,, \tag{16}$$

where p_0 and p_1 are calibration parameters and $\langle\eta_c\rangle$ is the average estimated mistag probability in the calibration sample. (This parameterization is chosen to minimize the correlation between p_0 and p_1.) Their values are given in Table 1 [2]. The systematic uncertainties are evaluated by comparing the tagging performance on various different decay channels (*e.g.* Fig 3 (right)), on B^+ and B^- samples separately and for different running periods.

p_0	p_1	$\langle\eta_c\rangle$
$0.384 \pm 0.003 \pm 0.009$	$1.037 \pm 0.04 \pm 0.07$	0.379

Table 1: Calibration parameters for the opposite side flavour tagging extracted from control samples as described in the text. The first error is statistical and the second systematic.

From the calibration parameters in Table 1 and the distribution of the estimated mistag probability in Fig. 4 the effective dilution of the $B_s^0 \to J/\psi\phi$ sample is estimated as

$$\left\langle \mathcal{D}^{\rm tag} \right\rangle_{\rm eff} \;=\; 0.277 \;\pm\; 0.006 \;\pm\; 0.016\,. \tag{17}$$

With an efficiency to obtain a tagging decision of $\varepsilon_{\rm tag} = (24.9 \pm 0.5)\%$, the effective tagging efficiency is $\varepsilon_{\rm tag}\mathcal{D}^2 = (1.91 \pm 0.23)\%$ [3]. The uncertainty in the dilution is dominated by

[2] The p_1 uncertainty was reported erroneously in the report version of September 27.

[3] These numbers were reported erroneously in the report version of September 27.

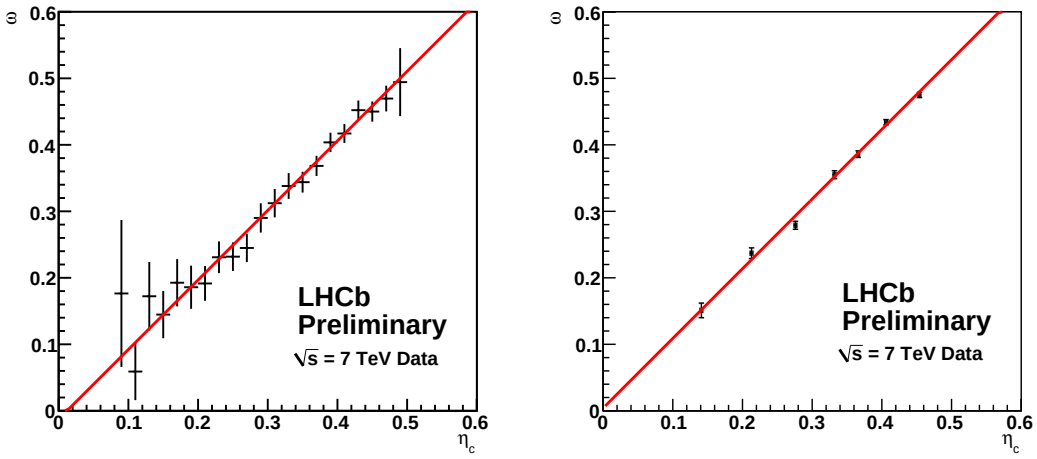

Figure 3: Measured OS mistag fraction (ω) as a function of estimated mistag probability (η_c) for background subtracted $B^+ \to J/\psi K^+$ candidates (left) and $B^0 \to D^{*-}\mu^+\nu_\mu$ candidates (right). The lines represent the result of the fit. The parameters of the fit to the $B^+ \to J/\psi K^+$ data are given in Table 1. The fit to the data gives consistent results.

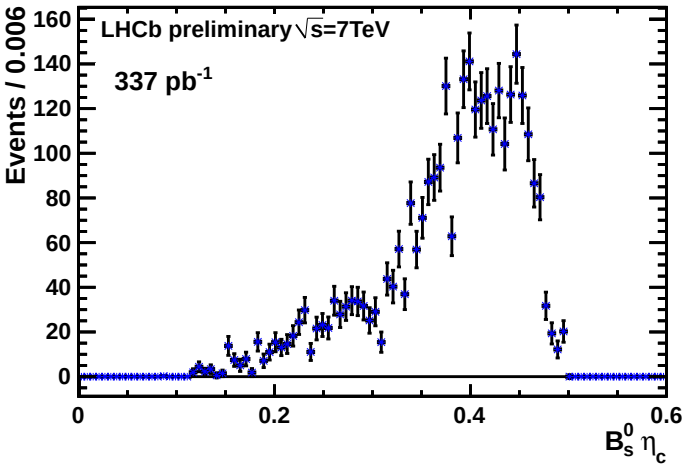

Figure 4: Distribution of calibrated OS mistag probability for $B_s^0 \to J/\psi\phi$ signal candidates.

the systematic uncertainties. However, as their evaluation is however statistically limited, we expect further improvement with a larger data sample.

The uncertainties from flavour tag calibration are included in the statistical uncertainties of the physics parameters presented in the next section by allowing the tagging calibration parameters to vary in the maximum likelihood fit within their known uncertainties. The uncertainty on the oscillation frequency is also included in the fit, by varying Δm_s constrained to the LHCb measurement of $17.63 \pm 0.11\,\mathrm{ps}^{-1}$ [18].

In the maximum likelihood fit we ignore a possible difference in mistag probability between B_s^0 and $\overline{B}_s^0$. This asymmetry is studied as part of the calibration procedure and included in the uncertainties on the calibration parameters. We also ignore the effects of a tagging efficiency asymmetry and a production asymmetry, *i.e.* a difference in the production cross sections of B_s^0 and $\overline{B}_s^0$ mesons. These effects are taken into account as part of the systematic uncertainty. Their contributions are found to be small.

2.3 Decay time resolution

To account for the finite decay time resolution of the detector, all time dependent functions in the PDF are convolved with a resolution model consisting of the sum of three Gaussians with a common mean. The parameters of the resolution model are determined from a fit to the prompt combinatorial background. We find that the $J/\psi \to \mu^+\mu^-$ component of the prompt background has a better resolution than the combinatorial $\mu^+\mu^-$ component. From studies on simulated data we expect that fake $B_s^0 \to J/\psi\phi$ candidates with a real prompt J/ψ are more representative for signal than purely combinatorial background. Therefore, the parameters of the resolution model are determined from a fit to the decay time distribution of $J/\psi \to \mu^+\mu^-$ component of the background, isolated using the sPlot technique. The decay time distribution with a curve representing the fit model is shown in Figure 5. The resolution parameters extracted from the fit are given in Table 2 where $\sigma_{1,2,3}$ are the RMS of each component, and f_2 (f_3) is the fraction of the second (third) component.

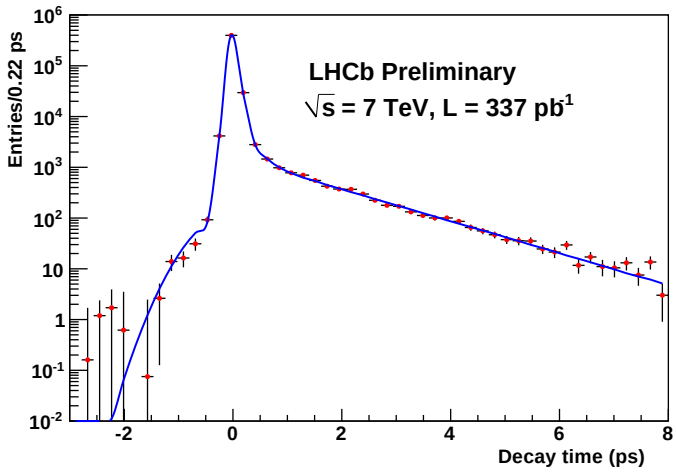

Figure 5: Decay time distribution of $B_s^0 \to J/\psi\phi$ candidates with a true $J/\psi \to \mu^+\mu^-$ obtained with the sPlot [21] technique using the reconstructed J/ψ mass as discriminating observable. The superimposed curve is the decay time model convolved with the resolution model. The model consists of a delta function for the prompt component and two exponentials with different decay constants, one of which represents the $B_s^0 \to J/\psi\phi$ signal.

σ_1 [fs]	σ_2 [fs]	σ_3 [fs]	f_2	f_3
43.4 ± 0.2	85.3 ± 1.1	513 ± 39	0.165 ± 0.007	0.0017 ± 0.0002

Table 2: Resolution parameters extracted from the fit explained in the text. The uncertainties are statistical only and highly correlated.

As with imperfections in the flavour tagging, the decay time resolution leads to a dilution of the oscillation amplitude [19]. For a oscillation frequency of $17.7\,\mathrm{ps}^{-1}$, the effective dilution for our sample is given by

$$\langle \mathcal{D}^{\mathrm{reso}} \rangle_{\mathrm{eff}} \;=\; 0.673 \;\pm\; 0.013\,, \tag{18}$$

which corresponds to an effective (single Gaussian) decay time resolution of approximately 50 fs.

Uncertainties in the dilution arise from differences in the resolution between signal events and the prompt background events that are used to extract the parameters of the resolution model. We estimate this uncertainty by studying the decay time resolution of $B_s^0 \to J/\psi\,\phi$ candidates in simulated signal events and prompt J/ψ events. We find that the effective resolution obtained from prompt J/ψ events is identical to that for signal events within about 1.2%. We also observe a small dependence of the resolution parameters on the selected decay time interval in the data, leading to an additional uncertainty of 1.1%. From this we derive a total systematic uncertainty in the effective decay time resolution of 2%. This uncertainty is taken into account directly in the maximum likelihood fit by introducing a floating parameter s that scales the width of each Gaussian component in the resolution function. The value of s is constrained to 1.00 ± 0.02.

2.4 Decay time acceptance

In this analysis we use events from two different types of triggers, namely either solely based on the signature of exclusive $J/\psi \to \mu^+\mu^-$ or additionally on tracks with high impact parameter. The $J/\psi \to \mu^+\mu^-$ triggers avoid any cuts that potentially bias the decay time distribution of the signal and provide about 86% of the signal candidates. On simulated events we find that this selection still leads to a shallow fall in acceptance at high decay times, which can be attributed to a reduction in track finding efficiency for tracks from very displaced vertices. This effect is parameterized using the simulation and accounted for in the likelihood fit.

The remaining 14% of signal candidates suffer additionally from a strong drop in efficiency at small decay times. The decay time acceptance is described with an empirical parameterization motivated by a Monte Carlo simulation that includes a full description of the trigger. The parameters are extracted from the data by comparing the decay time distribution of these events to that of events selected through the decay time unbiased $J/\psi \to \mu^+\mu^-$ triggers. The resulting acceptance curve is used in the likelihood fit.

2.5 Decay angle resolution and acceptance

The effect of the angular resolution on the decay angle distributions has been shown to be small [20] and is ignored in the PDF. Angular acceptance are obtained from Monte Carlo simulations and taken into account in the likelihood fit [16]. Differences between simulated and observed kaon momentum spectra are used to derive a systematic uncertainty on the angular acceptance. The resulting bias depends on the central value assumed for $\phi_s^{J/\psi\phi}$ and $\Delta\Gamma_s$. Within the 95% confidence region preferred by the data we find maximum deviations of 0.004 rad in $\phi_s^{J/\psi\phi}$ and 0.008 ps^{-1} in $\Delta\Gamma_s$. We have studied several different methods to treat the angular distribution of the background. Differences in the fit results are assigned to the uncertainty in the background description, and lead to a systematic uncertainty of 0.06 rad in $\phi_s^{J/\psi\phi}$ and 0.004 in $\Delta\Gamma_s$.

3 Results

The 2011 data set constitutes a sufficiently large sample of tagged signal events to constrain most physics parameters with near parabolic log-likelihood in the range $\pm 1\sigma$ (see *e.g.* Fig. 6). An exception holds for the strong phase $\delta_\parallel$. For the latter we estimate a 68% confidence level interval of $\delta_\parallel \in [3.01, 3.36]$ rad (statistical only). The extracted values for the remaining parameters, as well as estimated statistical and systematic uncertainties, are given in Table 3

Parameter	Value	Stat.	Syst.
Γ_s [ps^{-1}]	0.656	0.009	0.008
$\Delta\Gamma_s$ [ps^{-1}]	0.123	0.029	0.011
$\lvert A_\perp(0)\rvert^2$	0.238	0.015	0.011
$\lvert A_0(0)\rvert^2$	0.497	0.013	0.031
$\lvert A_s(0)\rvert^2$	0.041	0.016	0.019
$\delta_\perp$ [rad]	2.94	0.37	0.12
δ_s [rad]	3.00	0.36	0.12
$\phi_s^{J/\psi\phi}$[rad]	0.13	0.18	0.07

	Γ_s	$\Delta\Gamma_s$	$\phi_s^{J/\psi\phi}$	$\lvert A_\perp\rvert^2$	$\lvert A_0\rvert^2$
Γ_s	1.00	-0.30	0.12	0.28	-0.30
$\Delta\Gamma_s$		1.00	-0.08	-0.68	0.56
$\phi_s^{J/\psi\phi}$			1.00	0.11	-0.08
$\lvert A_\perp\rvert^2$				1.00	-0.32
$\lvert A_0\rvert^2$					1.00

Table 3: Left: Fitted values for the physics parameters (for one of the twofold solutions, see Eq 14) and their statistical and systematic uncertainties. Right: 5×5 correlation matrix for the statistical uncertainties on Γ_s, $\Delta\Gamma_s$, $|A_\perp(0)|^2$, $|A_0(0)|^2$ and $\phi_s^{J/\psi\phi}$.

The results on $\phi_s^{J/\psi\phi}$and $\Delta\Gamma_s$ are in good agreement with the Standard Model predictions [6]. We provide the world's most precise measurement of Γ_s and establish the first experimentally significant direct evidence for a non-zero $\Delta\Gamma_s$ value. Note that the strong phases are all consistent with zero or π.

The systematic uncertainties quoted in Table 3 account for uncertainties that are not directly treated in the maximum likelihood fit. A breakdown of the systematic uncer-

Source	$\phi_s^{J/\psi\phi}$[rad]	$\Delta\Gamma_s$ [ps^{-1}]
Description of background	0.06	0.004
Angular acceptances	0.004	0.008
z and momentum scale	–	0.002
Production asymmetry ($\pm$ 10%)	< 0.01	< 0.001
CPV in mixing & decay ($\pm$ 5%)	< 0.03	< 0.006
Quadratic sum	0.07	0.011

Table 4: Breakdown of the systematic uncertainties evaluated for $\phi_s^{J/\psi\phi}$and $\Delta\Gamma_s$.

tainty for $\phi_s^{J/\psi\phi}$ and $\Delta\Gamma_s$ is given in Table 4. The uncertainty is dominated by imperfect knowledge of the angular acceptances and the shape of the background. The largest contribution to the systematic uncertainty on Γ_s stems from the decay time acceptance.

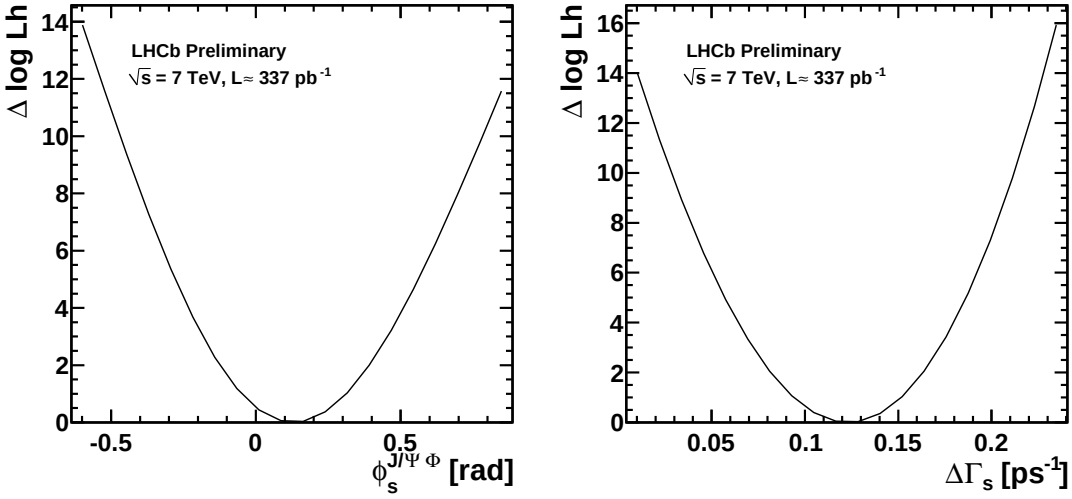

Figure 6: 1D likelihood profiles for $\phi_s^{J/\psi\phi}$(left) and $\Delta\Gamma_s$ (right).

Figure 7 shows the projection of the fitted PDF on the decay time and the transversity angle distributions for candidates with an invariant mass within $\pm$ 20 MeV/c^2 around the nominal B_s^0 mass. Figure 8 shows the 68.3%, 90% and 95% likelihood confidence level contours in the $\phi_s^{J/\psi\phi} - \Delta\Gamma_s$ plane including systematic uncertainties. The contours exhibit a symmetry due to the two-fold ambiguity in equation 14[4].

To evaluate the overall agreement of the PDF with the data in the multidimensional space we perform a measurement of goodness of fit based on the point-to-point dissimilarity test [22]. The p-value obtained for the five dimensional PDF on these data is 0.44.

From the unbinned likelihood fit to the angles and decay time distribution we extract a fraction of non-resonant K^+K^- S-wave of $|A_s^2(0)| = 0.041 \pm 0.016 \pm 0.019$ in a window of

[4]The second solution is displayed shifted by -2π in ϕ_s.

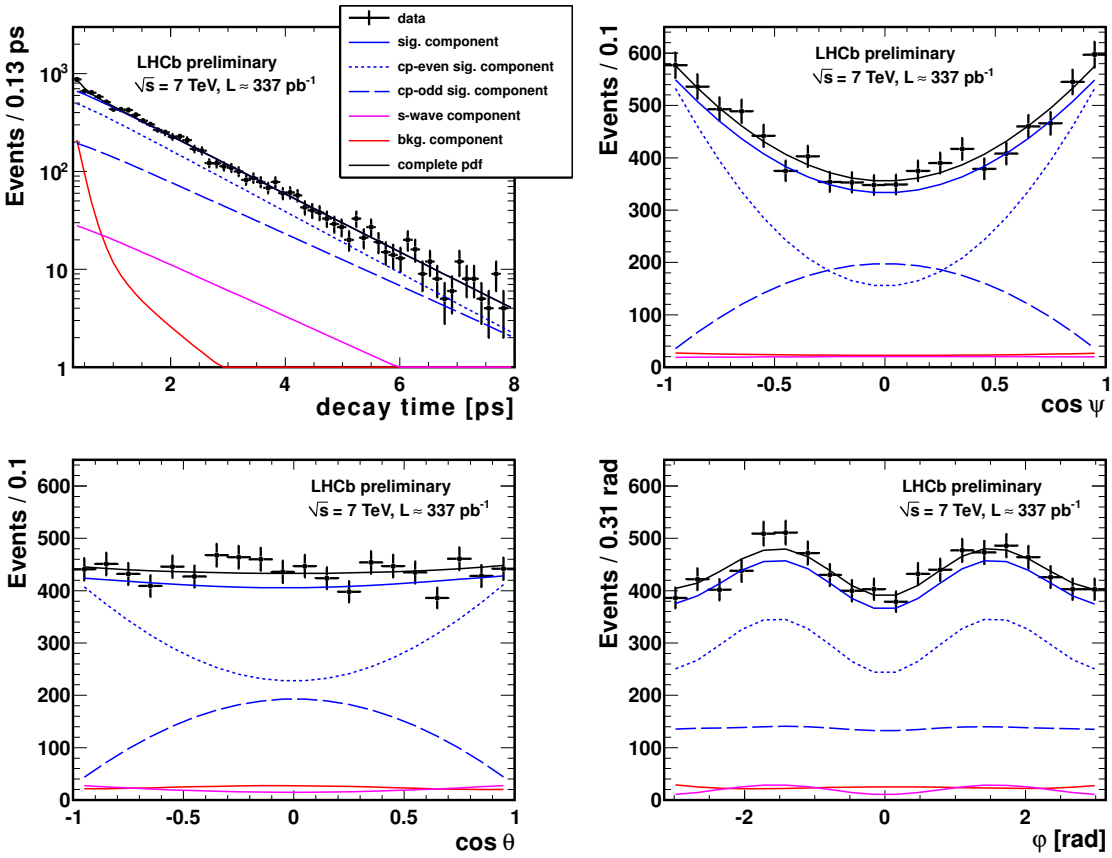

Figure 7: Data points overlaid with fit projections for the decay time and transversity angle distributions in as mass range of $\pm$ 20 MeV/c^2 around the reconstructed B_s^0 mass. The decay time acceptances applied to the signal component are analogously applied to the background decay time distributions. The total fit result is represented by the black line. The signal component is represented by the solid blue line; the dashed and dotted blue lines show the CP-odd and CP-even signal components respectively. The S-wave component is represented by the solid pink line. The background component is given by the red line.

$\pm$ 12 MeV around the ϕ mass. To illustrate the potential room for an S-wave contribution we show the K^+K^- invariant mass distribution in Figure 9 in a larger mass window. For this preliminary analysis we parameterize the distribution with a relativistic spin-1 Breit-Wigner on top of a non-resonant contribution ignoring the interference. The non-resonant component is modeled with a PDF $\mathcal{P}(m) \propto p_K(m)^\alpha$ where $p_K(m)$ is the momentum of a kaon in the K^+K^- rest frame and α is a free parameter. A curve representing the model is shown in blue for the sum and in red for the non-resonant component only. From this fit we extract a non-resonant contribution over the full mass range of about 5%, in agreement with the result from the angular analysis.

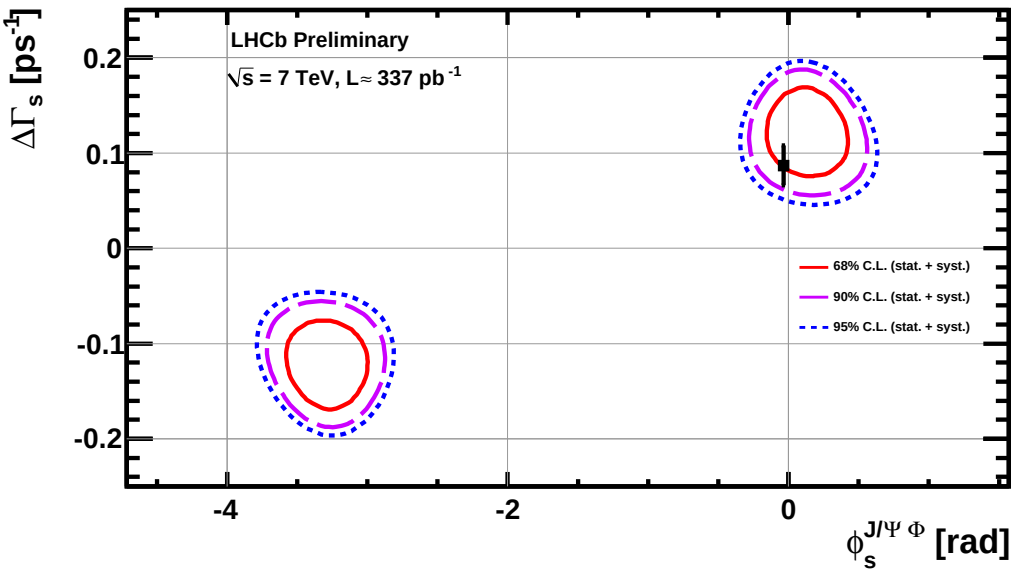

Figure 8: 2D likelihood confidence regions in the $\phi_s^{J/\psi\phi} - \Delta\Gamma_s$ plane. The black square corresponds to the theoretical predicted Standard Model value [4].

4 Conclusion

We have performed an analysis of the tagged, time-dependent, angular distribution of approximately 8276 ± 94 $B_s^0 \to J/\psi\phi$ candidates extracted from a sample of $337\,\text{pb}^{-1}$ of pp collisions collected during the 2011 LHCb run at $\sqrt{s} = 7\,\text{TeV}$. With an effective decay time resolution of 50 fs and an effective tagging efficiency of $\varepsilon_{\text{tag}}\mathcal{D}^2 = (2.08 \pm 0.26)\%$ we obtain the world's most precise measurement of $\phi_s^{J/\psi\phi}$ and Γ_s. Furthermore, we establish the first direct evidence for a non-zero value for $\Delta\Gamma_s$. We find two ambiguous solutions, one of which is

$$\begin{aligned} \phi_s^{J/\psi\phi} &= 0.13 \pm 0.18\ (\text{stat}) \pm 0.07\ (\text{sys})\ \text{rad}, \\ \Gamma_s &= 0.656 \pm 0.009\ (\text{stat}) \pm 0.008\ (\text{sys})\ \text{ps}^{-1}, \\ \Delta\Gamma_s &= 0.123 \pm 0.029\ (\text{stat}) \pm 0.011\ (\text{sys})\ \text{ps}^{-1}. \end{aligned}$$

This result is in good agreement with Standard Model predictions.

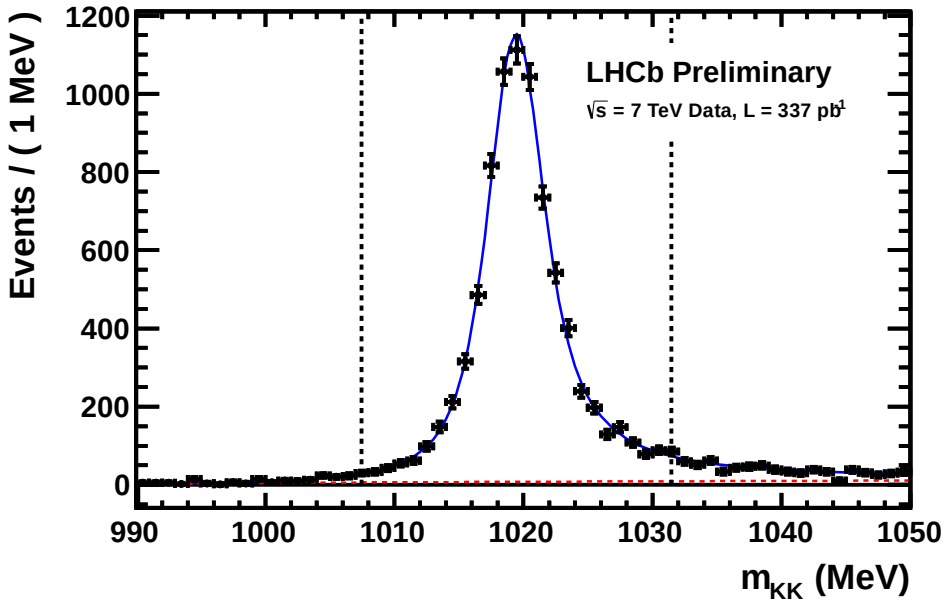

Figure 9: K^+K^- invariant mass distribution for $B_s^0 \to J/\psi\,\phi$ signal candidates isolated using the s-Plot technique. The fitted curve is described in the text. The black dotted lines indicate the K^+K^- invariant mass range used in the analysis.

References

[1] N. Cabibbo, Phys. Rev. Lett. **10** (1963) 531-533; M. Kobayashi, T. Maskawa, Prog. Theor. Phys. **49** (1973) 652-657.

[2] A. B. Carter, A. I. Sanda, Phys. Rev. **D23** (1981) 1567.; I. I. Y. Bigi, A. I. Sanda, Nucl. Phys. **B193** (1981) 85.

[3] A. S. Dighe, I. Dunietz and R. Fleischer, Eur. Phys. J. C **6** (1999) 647 [arXiv:hep-ph/9804253]; I. Dunietz, R. Fleischer and U. Nierste, Phys. Rev. D **63** (2001) 114015 [arXiv:hep-ph/0012219].

[4] A. Lenz *et al.*, Phys. Rev. D **83**, 036004 (2011) [arXiv:1008.1593 [hep-ph]].

[5] A. Lenz and U. Nierste, JHEP 0706 (2007) 072;

[6] A. Lenz and U. Nierste, arXiv:1102.4274 [hep-ph].

[7] See for example: Z. Ligeti, M. Papucci and G. Perez, Phys. Rev. Lett. 97, 101801 (2006); P. Ball and R. Fleischer, Eur. Phys. J. C **48** (2006) 413; A. Lenz, Phys. Rev. D 76, 065006 (2007); U. Nierste, Int. J. Mod. Phys. 22, 5986 (2008).

[8] The CDF Collaboration, public note CDF/ANAL/BOTTOM/PUBLIC/10206 (2010).

[9] The D0 Collaboration, D0 Conference note 6098-CONF (2010).

[10] S. Burdin (D0 Collaboration), "Measurements of CP violation in the B_s system at D0", talk given at the EPS'2011 conference, Grenoble, France, 20–27 July (2011).

[11] The LHCb Collaboration, "Tagged time-dependent angular analysis of $B_s^0 \to J/\psi\phi$ decays with $\sim 36\ pb^{-1}$", LHCb-CONF-2011-006.

[12] The LHCb Collaboration, "b-hadron lifetime measurements with exclusive $B \to J/\psi X$ decays reconstructed in the 2010 data", LHCb-CONF-2011-001.

[13] A. S. Dighe, I. Dunietz, H. J. Lipkin, J. L. Rosner, Phys. Lett. **B369**, 144-150 (1996). [hep-ph/9511363].

[14] S. Stone, L. Zhang, Phys. Rev. **D79** (2009) 074024. [arXiv:0812.2832 [hep-ph]].

[15] Y. Xie, P. Clarke, G. Cowan, F. Muheim, JHEP **0909** (2009) 074. [arXiv:0908.3627 [hep-ph]].

[16] The LHCb Collaboration, "Untagged angular analysis of $B_s^0 \to J/\psi\phi$ and $B^0 \to J/\psi K^{*0}$ with the 2010 data", LHCb-CONF-2011-002.

[17] The LHCb Collaboration, "Optimization and Calibration of the Tagging performances using 2010 data", LHCb-CONF-2011-003.

[18] The LHCb Collaboration, "Measurement of ΔM_s in $B_s^0 \to D_s(3)\pi$ decays using the 2010 data sample", LHCb-CONF-2011-005.

[19] H. G. Moser and A. Roussarie, "Mathematical methods for B0 anti-B0 oscillation analyses," Nucl. Instrum. Meth. A **384** (1997) 491.

[20] The LHCb Collaboration, "Roadmap for selected key measurements of LHCb.", LHCb-PUB-2009-029, arXiv:0912.4179

[21] M. Pivk and F. Le Diberder, "sPlot: a statistical tool to unfold data distributions", NIM A555 (2005) 356-369.

[22] M. Williams, "How good are your fits? Unbinned multivariate goodness-of-fit tests in high energy physics" JINST **5** (2010) P09004 [arXiv:1006.3019 [hep-ex]]